

Tryptanthrin exerts anti-breast cancer effects both *in vitro* and *in vivo* through modulating the inflammatory tumor microenvironment

QINGFANG ZENG^{1,2}
CAIRONG LUO^{1,2}
JUNLAE CHO³
DONNA LAI³
XIANGCHUN SHEN^{1,*}
XIAOYAN ZHANG^{1,2,*}
WEI ZHOU^{1,*}

¹ School of Pharmacy
Key Laboratory of Optimal
Utilization of Natural Medicine
Resources, Guizhou Medical
University, Guiyang 550025
Guizhou, China

² School of Basic Medical
Sciences, Guizhou Medical
University, Guiyang 550025
Guizhou, China

³ Faculty of Medicine and Life
Science, The University of
Sydney, NSW, 2006, Australia

Tryptanthrin is an indole quinazoline alkaloid from the indigo-bearing plants, such as *Isatis indigotica* Fort. Typically, this natural compound shows a variety of pharmacological activities such as antitumor, antibacterial, anti-inflammatory and antioxidant effects. This study was conducted to assess the antitumor activity of tryptanthrin in breast cancer models both *in vitro* and *in vivo*, and to explore the important role of the inflammatory tumor microenvironment (TME) in the antitumor effects of tryptanthrin. Human breast adenocarcinoma MCF-7 cells were used to assess the antitumor effect of tryptanthrin *in vitro*. MTT assay and colony formation assay were carried out to monitor the antiproliferative effect of tryptanthrin (1.56–50.0 $\mu\text{mol L}^{-1}$) on inhibiting the proliferation and colony formation of MCF-7 cells, respectively. The migration and invasion of MCF-7 cells were evaluated by wound healing assay and Transwell chamber assay, respectively. Moreover, the 4T1 murine breast cancer model was established to examine the pharmacological activity of tryptanthrin, and three groups with different doses of tryptanthrin (25, 50 and 100 mg kg^{-1}) were set in study. Additionally, tumor volumes and organ coefficients were measured and calculated. After two weeks of tryptanthrin treatment, samples from serum, tumor tissue and different organs from tumor-bearing mice were collected, and the enzyme-linked immunosorbent assay (ELISA) was performed to assess the regulation of inflammatory molecules in mouse serum. Additionally, pathological examinations of tumor tissues and organs from mice were evaluated through hematoxylin and eosin (H&E) staining. The expression of inflammatory proteins in tumor tissues was measured by immunohistochemistry (IHC) and Western blotting. Tryptanthrin inhibited the proliferation, migration and invasion of MCF-7 cells, up-regulated the protein level of E-cadherin, and down-regulated those of MMP-2 and Snail, as suggested by the MCF-7 cell experiment. According to the results from *in vivo* experiment, tryptanthrin was effective in inhibiting tumor growth, and it showed favorable safety without inducing the fluctuations of body mass and organ coefficient ($p > 0.05$). In addition, tryptanthrin also suppressed the expression levels of NOS1, COX-2 and NF- κB in mouse tumor tissues, and regulated those of IL-2, IL-10 and TNF- α in the serum of tumor cells-transplanted mice. Tryptanthrin exerted its anti-breast cancer activities through modulating the inflammatory TME both *in vitro* and *in vivo*.

Keywords: tryptanthrin, antitumor, inflammatory tumor microenvironment, epithelial-mesenchymal transition, natural medicine

Accepted June 21, 2020
Published online July 6, 2020

* Correspondence; e-mail: shenxiangchun@126.com; drxyzhang@126.com; drwzhou@126.com

Oncogenesis depends not only on the cellular oncogenic cascades but also on the “soil”, which refers to the inflammatory tumor microenvironment (TME) (1, 2). Inflammatory TME exists before the development of the cancer stem cells, which may serve as a precancerous micro-cellular circumstance that, in turn, promotes the pathogenesis of malignancies. Oncogenes and tumor suppressors are the factors that regulate the inflammatory pathways where the activation or suppression of precancerous cells is caused by recruiting immune cells and inflammatory mediators (like cytokines, chemokines and prostaglandins) to affect the TME (3–5). TME is a complex network system constituted by tumor cells, immune cells, extracellular matrix (ECM) and interstitial tissues (6). Inflammation may induce oncogenesis through promoting cell proliferation, growth and metabolism, and maintaining genomic stability. This also leads to epigenetic changes and abnormal activation of the subsequent genes (7, 8). The inflammatory TME exerts the dual functions of both anti-inflammatory and pro-inflammatory, whereas cytokines are classified as the anti-inflammatory factors (including IL-4, IL-10, TGF- β) and pro-inflammatory factors (such as IL-1, IL-6, IL-8, IL-12, IL-18, TNF- α) (9–13). Among them, proinflammatory cytokines directly or indirectly activate the key transcription factors that control the cell life cycle, differentiation, death, movement and migration through triggering a series of cascade signaling pathways (4, 14). In addition, inflammation also provides a sufficient environment for the epithelial-mesenchymal transition (EMT), as well as tumor metastasis and invasion. During tumorigenesis, the loss of cell adhesion, changes in cell morphology and cytoskeletal polarization, vascular lesions, migration, intravascular invasion and survival are all tightly associated with the EMT-related signaling pathways (15, 16). Notably, transforming growth factor- β 1 (TGF- β 1) is an effective EMT regulator that regulates various cellular functions, including tumor occurrence, development and ECM remodeling (17), and it is mainly used as EMT inducer in many experimental studies. Inhibiting or blocking EMT occurrence may become an effective approach to limit the proliferation of tumor cells. An increasing number of research results show that inflammation plays an important role in the pathogenesis of malignancies through affecting the immune functions, besides, it is associated with tumor invasion and metastasis, and participates in the pathogenesis of breast cancer (13). The untransformed mammary epithelial cells can be transformed into mesenchymal cells, subsequently promoting tumor growth and metastasis via the TME inflammatory mediators (17). Therefore, inhibition of the inflammatory TME may be used as a potential therapeutic strategy for breast cancer and a marker to screen the anti-breast cancer drug molecules.

Tryptanthrin is a natural indole quinazoline alkaloid, and its chemical name is indolo-[2,1-*b*]quinazoline-6,12-dione. It is first isolated and purified from the indigo-bearing plants (such as *Isatis indigotica* Fort., *Strobilanthes cusia* Ktze., *Polygonum tinctorium* Lour.). Notably, *Radix isatidis* (Banlangen), the root of *Isatis indigotica*, has been used as a famous traditional Chinese medicine in the Herbal Classic of Shen Nong and Compendium of Materia Medica, and it has been clinically applied in China for thousands of years (<http://bowuguan.bucm.edu.cn/kpzl/zyyzs/48187.htm>, www.yaofangwang.com/medicine-568562.html), *Indigo naturalis* (Qingdai) is a dark blue powder leaf extract of the same indigo-bearing plant, whereas tryptanthrin shows remarkable antiviral, antitumor, and anti-angiogenic effects (18–22). Our group has carried out systematic research on *Radix isatidis* and tryptanthrin in the previous study. Microbial fermentation and total chemical synthesis for tryptanthrin have also been published previously (23, 24). Tryptanthrin, together with its derivatives, may be potentially used as the innovative pharmaco-therapeutic agent with high efficacy and safety (18, 25–27). It is also reported that tryptanthrin demonstrated a protective effect on BV2 microglial cells,

which is achieved through inhibiting the lipopolysaccharide (LPS)-induced inflammation, and down-regulation of pro-inflammatory cytokines (such as TNF- α and IL-6) *via* the Nrf2/HO-1 and NF- κ B pathways. Additionally, it ameliorates dextran sodium sulfate (DSS)-induced colitis in mice (28, 29). In our previous study, tryptanthrin is found to inhibit the proliferation of human breast cancer MCF-7 cells, and the underlying mechanism of action may be related to the activation of the MAPK signaling pathways. However, the effect of tryptanthrin on the inflammatory TME in breast cancer has not been investigated so far, and a few of the previous studies indicate that tryptanthrin has anti-inflammatory activity and inhibits breast cancer cell proliferation *in vitro* (30–32). Therefore, we hypothesize that tryptanthrin exerts its anti-breast cancer effects by modulating the inflammatory TME both *in vivo* and *in vitro*. To verify this hypothesis, the current study was carried out to examine the effects of tryptanthrin on the migration and invasion of human breast cancer MCF-7 cells and the post-transcriptional activation of EMT associated proteins *in vitro*. Further, the effects of tryptanthrin on modulating the inflammatory molecules and proteins, and the pathological changes in tumor tissues and organs were examined using tumor-bearing mice. Therefore, this study aimed to explore the mechanisms of action by which tryptanthrin exerted its antitumor effects through modulating the inflammatory TME both *in vitro* and *in vivo*.

EXPERIMENTAL

Chemicals

Tryptanthrin (purity > 99.0 %) was chemically prepared in our laboratory C-2-14 of School of Pharmacy, Guizhou Medical University, according to the reported method (33), the detected spectral data of tryptanthrin is as follows (Fig. 1): yellow powder, C₁₅H₈N₂O₂, ¹H NMR (400 MHz, CDCl₃) δ : 8.63 (d, *J* = 8.1 Hz, 1H, Ar-H), 8.44 (dd, *J* = 7.9, 1.3 Hz, 1H, Ar-H), 8.04 (d, *J* = 8.1 Hz, 1H, Ar-H), 7.92 (d, *J* = 7.5 Hz, 1H, Ar-H), 7.86 (td, *J* = 7.8, 1.5 Hz, 1H, Ar-H), 7.79 (td, *J* = 7.9, 1.3 Hz, 1H, Ar-H), 7.68 (m, 1H, Ar-H), 7.43 (t, *J* = 7.5 Hz, 1H, Ar-H). ¹³C NMR (101 MHz, CDCl₃) δ : 182.79, 158.29, 146.77, 146.51, 144.49, 138.50, 135.34, 130.91, 130.45, 127.73, 127.40, 125.61, 123.89, 122.08, 118.15. HSMS calcd for C₁₅H₈N₂O₂ (M+H)⁺ 249.0663, found 249.0659.

Cell lines and animals

4T1 cell line and MCF-7 cell line were successively purchased from Wuhan Yipu Biotechnology Company for two cell passages. 4T1 cells were maintained in 1640 medium supplemented with 10 % fetal bovine serum (FBS), 100 U mL⁻¹ penicillin, and 100 μ g mL⁻¹ streptomycin in an incubator under 37 °C and 5 % CO₂ conditions. Meanwhile, MCF-7 cells were cultivated in DMEM medium containing 10 % FBS, 100 U mL⁻¹ penicillin, and 100 μ g mL⁻¹ streptomycin. The 4-6-week-old adult Bal b/c female mice weighing 18–22 g were purchased from the Experimental Animal Center of Guizhou Medical University (Animal certificate number: SCXK (Beijing) 2016-0002).

Cell viability assay

MCF-7 cells were seeded into 96-well plates at a density of 1.0 \times 10⁵ cells mL⁻¹, and cultured in a cell incubator at 37 °C and 5 % CO₂ conditions. Then, the cells were treated

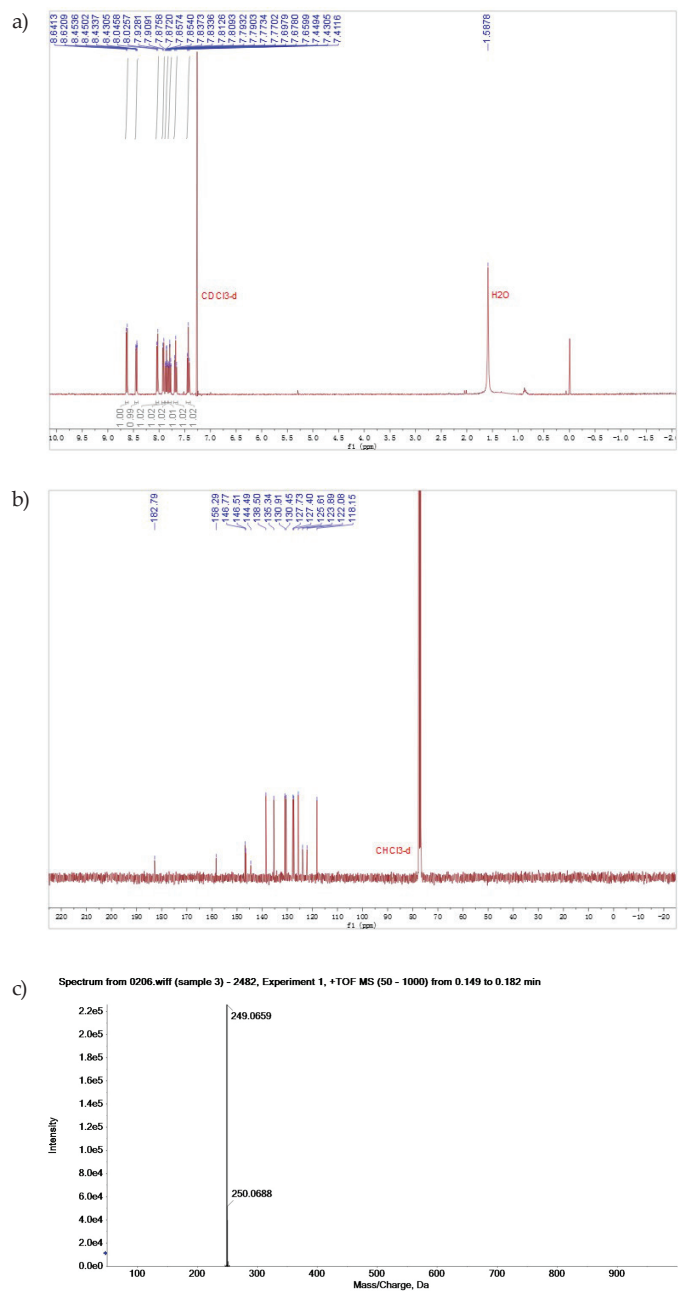


Fig. 1. a) ¹H NMR spectrum, b) ¹³C NMR spectrum and c) high-resolution mass spectrum of tryptanthrin.

with different concentrations of tryptanthrin (1.56, 3.13, 6.25, 12.5, 25.0, 50.0 $\mu\text{mol L}^{-1}$) for 24, 48 and 72 h, respectively. Afterward, 15 μL of 5 % MTT solution was added into each well for slight mixing, and the supernatant was discarded after continuous culture at 37 °C for 4 h. Subsequently, 150 μL DMSO was added into each well, and the plate was shaken at room temperature for 10 min to dissolve crystals. The experiments were repeated at least three times, the absorbance (OD) value was measured using the microplate reader at the wavelength of 490 nm, and the average value was calculated based on the experimental data of each group.

Cell colony-forming assay

MCF-7 cells were plated into the 6-well plate at a density of 250 cells mL^{-1} and treated with either tryptanthrin at 6.25, 3.13 and 1.56 $\mu\text{mol L}^{-1}$ or left untreated as the blank control group. Three wells were set for each treatment. After 2 weeks of culture, colonies containing at least 50 cells were stained with Giemsa, photographed and counted. The experiment was repeated at least three times.

H&E staining

A little amount of culture medium was dropped into the 24-well plate, and then the 24-well plate dedicated cell round-glass crawling slide (WHB-24-CS, ID 14mm, Shanghai Wohong Biotechnology) was placed horizontally in each well of the 24-well plate. The MCF-7 cell concentration was adjusted to 1.0×10^5 cells mL^{-1} , and then 600 μL cell solution was added dropwise onto the glass slide surface. After the cell adhesion to the slide, the supernatants were removed, and the tryptanthrin-containing (6.25, 12.5, 25.0 $\mu\text{mol L}^{-1}$) culture medium was added to further culture the MCF-7 tumor cells on the cell-adhered glass slides at 37 °C for 24 h. Then these glass slides were taken out, then cells were washed twice with PBS, fixed with 95 % ethanol, and washed with PBS again. Later, cells on the glass slides were stained with hematoxylin for 5 min and washed with PBS; then, the glass slides were immersed into the 1 % hydrochloric acid alcohol solution to differentiate cells for 10 s and washed with PBS again. Finally, these slides were transferred into the eosin dye solution for 6 min, washed with PBS, blow/air dried, and photographed under an optical microscope to obtain the results.

Wound healing assay

A wound healing assay was carried out to detect the migration of tumor cells, MCF-7 cells were inoculated into six-well plates, and the assay was initiated when the cells reached 80–90 % confluence. Tumor cells in the model group were treated with 5 $\mu\text{g L}^{-1}$ TGF- β 1 (Lot no. 0218209-1, PeproTech) for 48 h. Then, a scratch was made in each well of six-well plates using a 200- μL pipette tip, and the plates were washed twice with PBS. Five cell experimental groups were set in this experiment, including a blank control group, model group, as well as high, medium and low concentration of tryptanthrin groups. Of them, cells in model group were treated with TGF- β 1 (containing 1 % FBS); those in the three different concentration tryptanthrin groups were treated with TGF- β 1+6.25 $\mu\text{mol L}^{-1}$ tryptanthrin, TGF- β 1+3.13 $\mu\text{mol L}^{-1}$ tryptanthrin and TGF- β 1+1.56 $\mu\text{mol L}^{-1}$ tryptanthrin, respectively. Later, cells in each group were photographed in the same position after 0 and 24 h of the above-mentioned treatments, respectively, and the scratch width was measured with the ImageJ software.

Also, the scratch healing rate was calculated according to the following formula to reflect the migration capacity of tumor cells, and the experiment was repeated at least three times.

$$\text{Scratch healing rate} = \frac{\text{Scratch width}_{(0\text{h})} - \text{Scratch width}_{(24\text{h})}}{\text{Scratch width}_{(0\text{h})}}$$

Transwell chamber assay

Transwell chamber assay on the invasion of tumor cells, tumor cells were inoculated into the six-well plates, and five cell experimental groups were set in this experiment, which were the blank control group, the model group ($5 \mu\text{g L}^{-1}$ TGF- β 1), as well as high, medium and low concentrations of tryptanthrin groups. Specifically, cells in these three different concentration tryptanthrin groups were treated with TGF- β 1+ $6.25 \mu\text{mol L}^{-1}$ tryptanthrin, TGF- β 1+ $3.13 \mu\text{mol L}^{-1}$ tryptanthrin and TGF- β 1+ $1.56 \mu\text{mol L}^{-1}$ tryptanthrin, respectively, for 24 h. Subsequently, $80 \mu\text{L}$ Matrigel (1:11 dilution, Lot no. 7205008, Corning) was added into the insert of each 24-well Transwell plate (Lot no. 25717024, Corning) to form the Matrigel layer on the insert membrane; then, all the above-treated inserts were maintained in a clean bench, and air-dried under the hood without UV light. Subsequently, cells were dissociated and diluted to 5×10^5 cells mL^{-1} , then $200 \mu\text{L}$ cell suspension was seeded into each 24-well Transwell plate coated with Matrigel, and $600 \mu\text{L}$ culture medium containing 10 % FBS was added to the lower layer of each 24-well Transwell plate. Following incubation for 24 h at 37°C , the culture medium in each well was discarded, the upper layer was washed twice with PBS, then both cells and Matrigel outside the permeable membrane were scraped off with sterilized cotton, and tumor cells invading the membrane were fixed with methanol and stained with crystal violet. Five random fields of view (FOV) were selected from each membrane of the 24-well Transwell plates under the microscope, and photos were taken to count the invading cells.

Western blotting

This assay was conducted in the 6-well plates supplemented with MCF-7 tumor cells. Five cell experiment groups were set, including the blank control group, the model group treated with $5 \mu\text{g L}^{-1}$ TGF- β 1 for 48 h, and three different concentrations of tryptanthrin-treated groups with TGF- β 1+ $25 \mu\text{mol L}^{-1}$ tryptanthrin, TGF- β 1+ $12.5 \mu\text{mol L}^{-1}$ tryptanthrin, and TGF- β 1+ $6.25 \mu\text{mol L}^{-1}$ tryptanthrin, respectively. After tryptanthrin treatment for 24 h, all cells were washed twice with the 4°C PBS and collected by centrifugation. The cellular proteins were extracted using the Nuclear and Cytoplasmic Protein Extraction Kit (Lot no. 050318180716, Shanghai Beyotime Biotechnology), and the cellular protein concentrations were determined using the BCA protein concentration determination kit (Lot no. 20180816, Beijing Solarbio). After sodium dodecyl sulfate-polyacrylamide gel electrophoresis (SDS-PAGE) vertical plate electrophoresis, the membranes were electrically transferred onto the polyvinylidene fluoride (PVDF) membrane (Lot no A16954280, GE Healthcare), sealed with 5 % skimmed milk powder for 1 h, and washed with TBST for 5 min three times. Subsequently, the membranes were incubated with E-cadherin (1:1000 dilution, Lot no. 3195T, Cell Signaling Technology), Snail (1:1000 dilution, Lot no. 3879T, Cell Signaling Technology), MMP-2 (1:1000 dilution, Lot no. GR319128-3, Abcam) and GAPDH (1:8000 dilution, Lot no.

10494-1-AP, Wuhan Sanying) antibodies overnight at 4 °C. Then, the membranes were washed with TBST three times, and then incubated with corresponding horseradish peroxidase (HRP)-labeled secondary antibody (1:5000 dilution, Lot no. 134658, Beijing Zhongshan Goldenbridge Biotechnology) for 2 h at room temperature. Later, the immunolabeled bands were visualized using the Immobilon ECL Western HRP substrate (Lot no. 1735601, Millipore). Digital images of the blots were photographed by the ChemiDoc XRS+ system and analyzed *via* the Image Lab Software (Bio-Rad Laboratories). The results were normalized to those of GAPDH, and data from three independent experiments were analyzed.

Establishment of 4T1 mouse breast cancer model

All Bal b/c mice were housed at the Experimental Animal Laboratory of School of Basic Medical Sciences, Guizhou Medical University. The experimental procedures and protocols were reviewed and approved by the Animal Care and Use Committee of Guizhou Medical University and carried out in strict accordance with the Guide for the Care and Use of Laboratory Animals. 0.1 mL of 1×10^6 mL⁻¹ well-grown murine breast cancer 4T1 cell suspension was injected into the right forelimb armpit of each SPF female Bal b/c mouse. These model mice were randomly divided into six groups when the tumor size grew to about 100 mm³ with 9 mice in each experimental group. Groups included were normal control group, model group (normal saline, NS), model group (0.5 % CMC-Na, sodium carboxymethyl cellulose), positive control group (40 mg kg⁻¹ cyclophosphamide), as well as high, medium and low concentration tryptanthrin groups (100.0, 50.0 and 25.0 mg kg⁻¹). The tryptanthrin solutions were administered through oral gavage to mice once daily for a total of 13 consecutive days. Then, the physical conditions and mental state of test mice were observed and recorded, the longest diameter (*a*) and the shortest diameter (*b*) of each tumor were measured with the vernier caliper daily, and the formula for calculating the tumor volume (*V*) was as follows, $V = \frac{1}{2} \times ab^2$.

Animal tissue harvesting

After continuous tryptanthrin administration for 13 days, the experimental mice were anesthetized to collect blood samples from the inferior vena cava. Meanwhile, the serum samples were obtained by low-temperature & low-speed centrifugation and preserved at -80 °C for subsequent ELISA. Afterward, the mice were sacrificed by cervical dislocation, and tumor, liver, spleen and lung were dissected from each mouse, divided into multiple parts, and finally stored in the -80 °C refrigerator for subsequent analyses. The computational formula of the organ coefficient was as follows:

$$\text{Organ coefficient} = \text{Organ mass} / \text{Body mass} \times 100 \%$$

ELISA

The IL-2, IL-6, IL-10, IL-12 and TNF- α levels in mouse serum were measured by the specific ELISA system kits (Lot no. 201808, Shanghai Jianglai Biology) in accordance with manufacturer instructions. The nonspecific binding signal was obtained after the incubation of serum samples and diluted into the appropriate buffer solution in the absence of the capture antibody. The experiments were repeated three times.

H&E staining of tumor tissues and organs

Pathological changes in tumor tissues and organs from tumor-bearing mice were observed by means of H&E staining. In brief, tumor tissues and organs were fixed with the 4 % paraformaldehyde solution, embedded in paraffin, and sliced into the 4 μm paraffin sections, followed by further deparaffinage and staining according to the standard operational procedure of H&E. Thereafter, the sections were subjected to methanol gradient dehydration, xylene transparentizing, and sealing with neutral gum. The results of H&E staining were presented in the electronic photos through microscopic analysis and photographs.

IHC and Western blotting of tumor tissues

IHC experiment was conducted to measure the protein levels of NOS1 and COX-2 in tumor tissues from tumor-bearing mice. Similarly, the tumor tissues were fixed with 4 % paraformaldehyde solution, dehydrated, embedded in paraffin, sliced and other operational steps. The IHC tissue sections were incubated with primary antibody solution and then secondary antibody solution at room temperature in dark. Afterwards, DAB staining, hematoxylin counterstaining, staining and sealing of the tested tissue sections were completed in succession. The IHC staining results were collected finally.

Mouse tumor tissues were cut into pieces, lysed in the tissue-lysate solution (1 mg:10 μL , RIPA, Lot no. 20170712, Solarbio), and homogenized with the glass homogenizer. Then, tissue protein concentrations were determined through the BCA method, and the NF- κB p65 protein expression in the tumor tissues from tumor-bearing mice was analyzed by Western blotting. Following tumor tissue lysis, the proteins were resolved by SDS-PAGE, transferred onto the PVDF membranes, and incubated with primary and secondary antibodies. In this experiment, the anti-NF- κB p65 (1:1000 dilution, Lot no. 8242S, Cell Signaling Technology) and anti-GAPDH primary antibodies were used. The protein bands were visualized by chemiluminescence and quantified through densitometry using Image Lab Software. The results were normalized to those of GAPDH, and the data from three independent experiments were analyzed.

Statistical analysis

The SPSS 22.0 software was adopted for statistical analysis, and the statistical significance was compared using Student's *t*-test or one-way analysis of variance (ANOVA), followed by post-hoc test. $p < 0.05$ indicated statistical significance. All results are expressed as mean \pm SD.

RESULTS AND DISCUSSION

Tryptanthrin inhibited the proliferation and colony formation of MCF-7 cells

Human breast cancer MCF-7 cells were treated with different concentrations of tryptanthrin for 24, 48 and 72 h, respectively. The curves regarding cell proliferation inhibition rates are shown in Fig. 2a. As observed, the inhibition rates of the low, medium and high concentration tryptanthrin groups remarkably increased ($*p < 0.05$, $**p < 0.01$ or $***p < 0.001$) in a time-

and concentration-dependent manner. Particularly, when MCF-7 cells were treated with 50.0 $\mu\text{mol L}^{-1}$ tryptanthrin for 72 h, the proliferation rate of MCF-7 cells suffered from the most significant decrease ($***p < 0.001$). In the colony formation assay, the number of colonies formed in MCF-7 cells treated with tryptanthrin at 6.25, 3.13 and 1.56 $\mu\text{mol L}^{-1}$ was dramatically lower than that in the blank control group (Fig. 2b). These results clearly demonstrated that tryptanthrin exerted the antitumor activity on MCF-7 cells partially by decreasing cell viability and inhibiting proliferation. Results of H&E staining revealed that the *in vitro* morphologic changes in MCF-7 cells, induced by tryptanthrin treatment, were more pronounced than those in the blank control group. Typically, good cell adherence, reddish cytoplasm and irregular spindle shape were the main characteristics of MCF-7 cells. After tryptanthrin treatment and killing of tumor cells, the number of MCF-7 cells has decreased, along with poor cell adherence, darkened nuclei, disappeared cell membrane, and diffused cytoplasm (Fig. 2c). These cellular morphologic changes demonstrated the favorable antitumor effect of tryptanthrin.

Tryptanthrin blocked migration and invasion of MCF-7 cells

The tumor cell mobility in TGF- β 1 induced model group substantially increased compared with that in the blank control group ($^{\#}p < 0.05$) (Fig. 3). After treatment with 3.13 and 6.25 $\mu\text{mol L}^{-1}$ tryptanthrin solutions, the tumor cell mobilities in tryptanthrin groups outstandingly decreased relative to that in the model group ($^{\#}p < 0.05$, $^{**}p < 0.01$). Fig. 3 shows the microscopic photographs ($\times 200$) and scratch healing rates of MCF-7 tumor cells in the three tryptanthrin concentration groups. The results show what tryptanthrin had greatly inhibited the migration of MCF-7 tumor cells *in vitro*. In the tumor cell invasion experiment, the high dose tryptanthrin (6.25 $\mu\text{mol L}^{-1}$) had maximally reduced the invasion of MCF-7 tumor cells, with the smallest number of invading cells ($***p < 0.001$, Fig. 4); therefore, the tryptanthrin concentration was in direct proportion to the number of invading tumor cells. Our results indicated that tryptanthrin dramatically blocked the migration and invasion of MCF-7 tumor cells.

Tryptanthrin reversed EMT-associated E-cadherin, MMP-2 and Snail

EMT is an embryonic procedure known to participate in breaking down the cell adhesion complexes and enhancing cell migration and invasion. Cancer cells with EMT show higher aggressiveness, stronger invasiveness, obvious stem cells-like characteristics, and higher anti-apoptosis capacity (34). E-cadherin initiates a series of signal transduction pathways and a major cell framework recombination process, and the deletion of E-cadherin is considered as a critical step in tumor and EMT development. The post-transcriptional activation of E-cadherin is an important factor to predict the prognosis for breast cancer, since this protein is considered as one of the EMT marker proteins. Hence, we evaluated the expression of E-cadherin in MCF-7 cells induced by TGF- β 1 in this study. The results suggested the reduction of the E-cadherin protein expression in the model group (MCF-7 cells treated with TGF- β 1; $^{\#}p < 0.05$). However, when cells were treated with tryptanthrin, the E-cadherin protein levels in cells treated with 6.25, 12.5, and 25.0 $\mu\text{mol L}^{-1}$ tryptanthrin had increased ($^{\#}p < 0.05$). Furthermore, the protein expression levels of MMP-2 and Snail in MCF-7 cells induced by TGF- β 1 were markedly upregulated ($^{\#}p < 0.05$). After tryptanthrin treatment, the protein levels of MMP-2 and Snail in 6.25, 12.5 and 25.0 $\mu\text{mol L}^{-1}$ tryptanthrin groups were remarkably downregulated ($^{\#}p < 0.05$, $^{**}p < 0.01$, Fig. 5). The above results indicated that tryptanthrin suppressed the EMT process to achieve the anti-tumor effect.

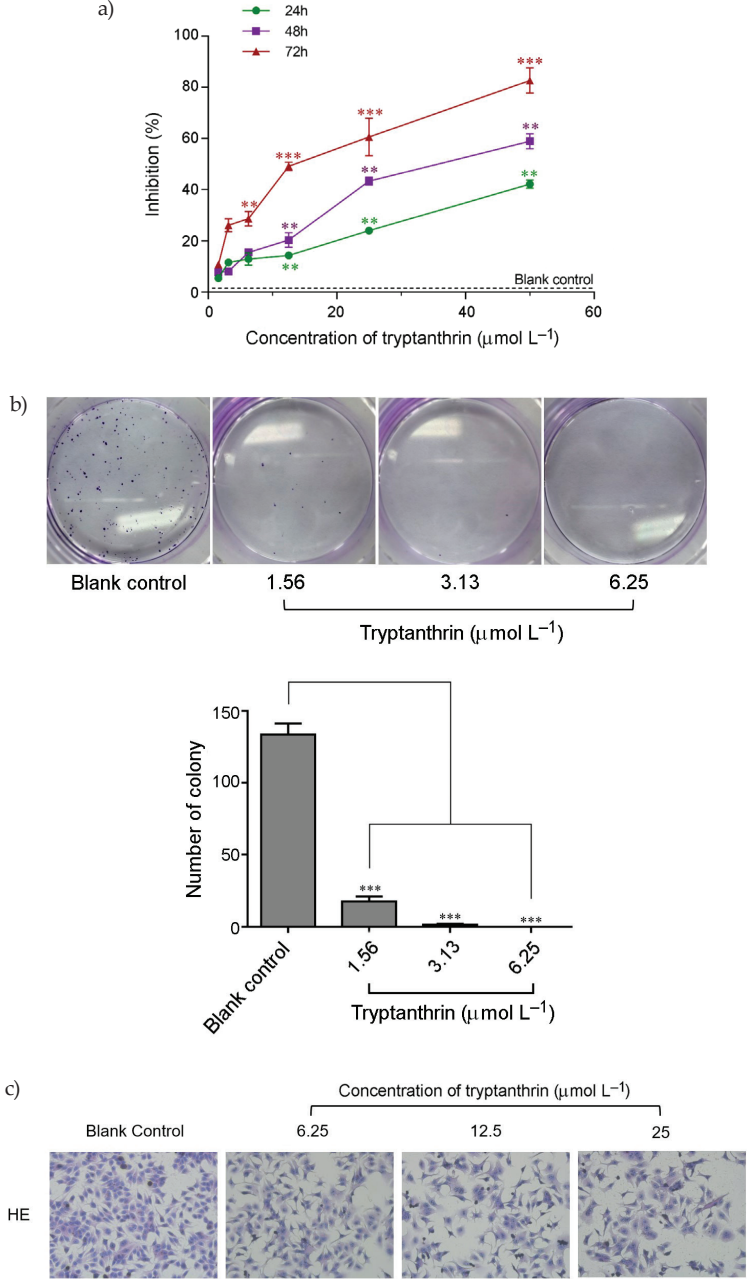


Fig. 2. a) Inhibitory effect of tryptanthrin on MCF-7 tumor cell proliferation, b) the number of MCF-7 cells' colony formations of and c) HE-stained optical microscopic photographs ($\times 200$) of tryptanthrin-treated MCF-7 cells (compared to the blank control group, $*p < 0.05$, $**p < 0.01$, $***p < 0.001$, $n = 6$).

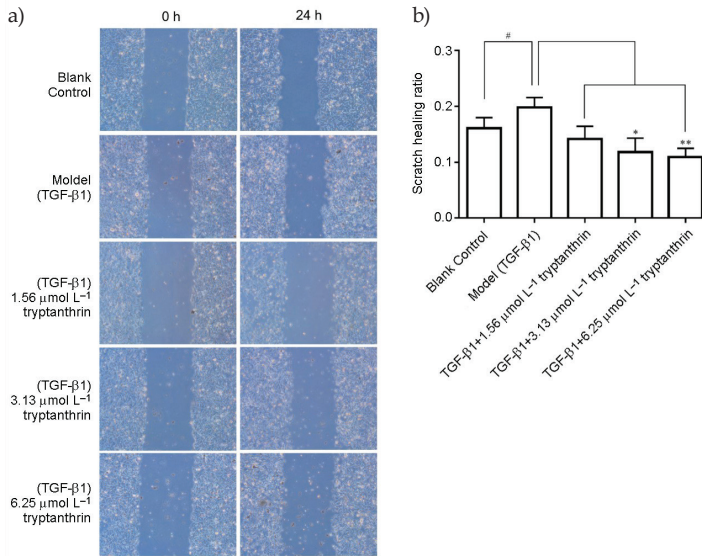


Fig. 3. a) The optical microscopic photographs ($\times 200$) and b) scratch healing rates of the effect of different tryptanthrin concentrations on the migration of MCF-7 tumor cells (compared to blank control group, $^{\#}p < 0.05$; compared to the model group, $^*p < 0.05$, $^{**}p < 0.01$, $n = 6$).

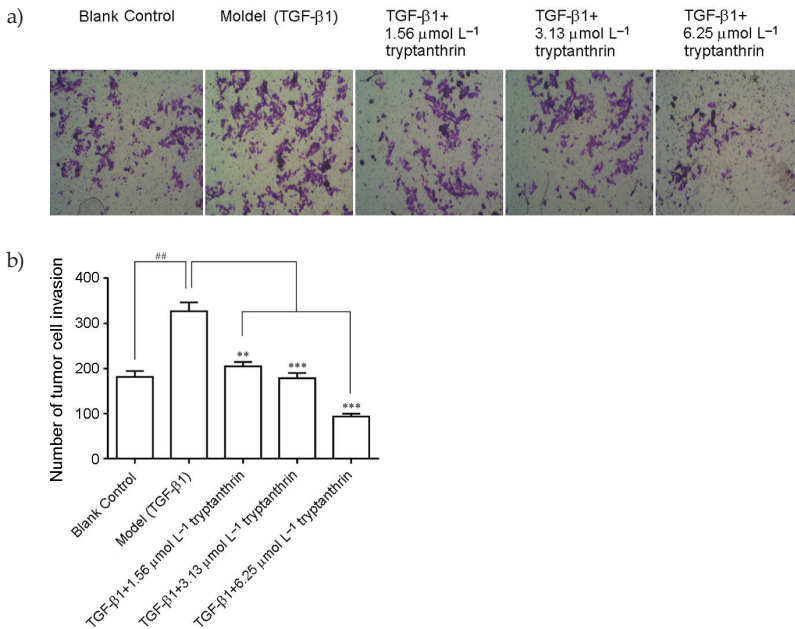


Fig. 4. a) The optical microscopic photographs ($\times 200$) and b) the quantized histograms of tumor cells after cell invasion after the treatment with different concentrations of tryptanthrin (compared to normal control group, $^{\#}p < 0.01$; compared to the model group, $^{**}p < 0.01$, $^{***}p < 0.001$, $n = 6$).

Effects of tryptanthrin on body mass, organ coefficients and tumor growth in tumor-bearing mice

The mental state of all tested mice was reflected indirectly through observing their daily food intake, physical strength and normal activity, and comparing the differences between distinct groups. The mice in experimental groups after tryptanthrin treatment had a better appetite and a greater range of limb motion than those in the morbid model group. The mean body mass of tumor-bearing mice was not evidently affected by tryptanthrin at different doses on the 13th day after tryptanthrin administration, and it showed a normal upward trend compared with the 19.16 ± 1.35 g of the model group (0.5 % CMC-Na) or 19.68 ± 1.04 g of the model group (NS). In sharp contrast to the positive group, the mean body mass of tumor-bearing mice given oral administration of 40 mg kg⁻¹ cyclophosphamide for 13 days was 17.0 ± 1.43 g, which was significantly reduced (Fig. 6). Besides, the organ coefficient of tumor-bearing mice is another effective physiological index. There were no significant differences in the coefficients of the liver, spleen, lung and kidney between the 100.0, 50.0, 25.0 mg kg⁻¹ tryptanthrin groups and the model groups ($p > 0.05$). Similarly to the changes in mass mentioned above, the organ coefficients of the liver, spleen, lung and kidney in the positive group were reduced (Fig. 7), especially for the coefficients of lung and kidney ($*p < 0.05$), as well as spleen ($**p < 0.01$).

Tumor growth in the tumor-bearing mice of different groups was investigated, and the change curves of tumor volume during the treatment period were collected, as summarized in Fig. 8a. The tumor volumes in 100.0, 50.0, 25.0 mg kg⁻¹ tryptanthrin-treated groups at the same treatment time were smaller than those in the two model groups, and the antitumor efficacy of 100.0 mg kg⁻¹ tryptanthrin was quite remarkable, which was only second to the positive drug-cyclophosphamide in this study. Fig. 8b shows the morphologic changes in breast cancer tissues from tumor-bearing mice treated with tryptanthrin. As shown by the results, different concentrations of tryptanthrin exhibited *in vivo* antitumor activities to various degrees; additionally, the data from model group and positive group testified the successful establishment of the *in vivo* tumor model, thus confirming the reliability of *in vivo* anti-tumor effect of tryptanthrin.

Tryptanthrin regulated IL-2, IL-6, IL-10, IL-12 and TNF- α levels in tumor-bearing mice

The serum IL-2 and TNF- α levels of tumor-bearing mice in 100.0, 50.0, 25.0 mg kg⁻¹ tryptanthrin-treated groups and the positive group had increased in comparison to those in the model group (0.5 % CMC-Na) ($*p < 0.05$, $**p < 0.01$). To be specific, the IL-2 levels in 100.0 and 50.0 mg kg⁻¹ tryptanthrin-treated groups were 1.93 and 1.67 as high as that in the model group; while the TNF- α level in 100.0 mg kg⁻¹ tryptanthrin group was 1.37 times of that in model group. As a soluble leukocyte stimulating factor released by T cells, IL-2 is considered as a growth factor of T cells and natural killer cells, which exerts an anti-tumor role through promoting the activities of these cells (35, 36). Relevant studies demonstrate that IL-2 has considerable therapeutic efficacy in the treatment of cancer. TNF- α induces tumor apoptosis and mediates the occurrence of chronic inflammation, thus initiating the development of the malignant tumor. The serum IL-10 levels in tumor-bearing mice from tryptanthrin-treated groups were almost identical to those in the normal group, whereas the levels in the model group (0.5 % CMC-Na) were relatively high compared to the normal group ($#p < 0.05$). IL-10 is reported to promote the tumor immune escape by reducing the anti-tumor immune response in the TME,

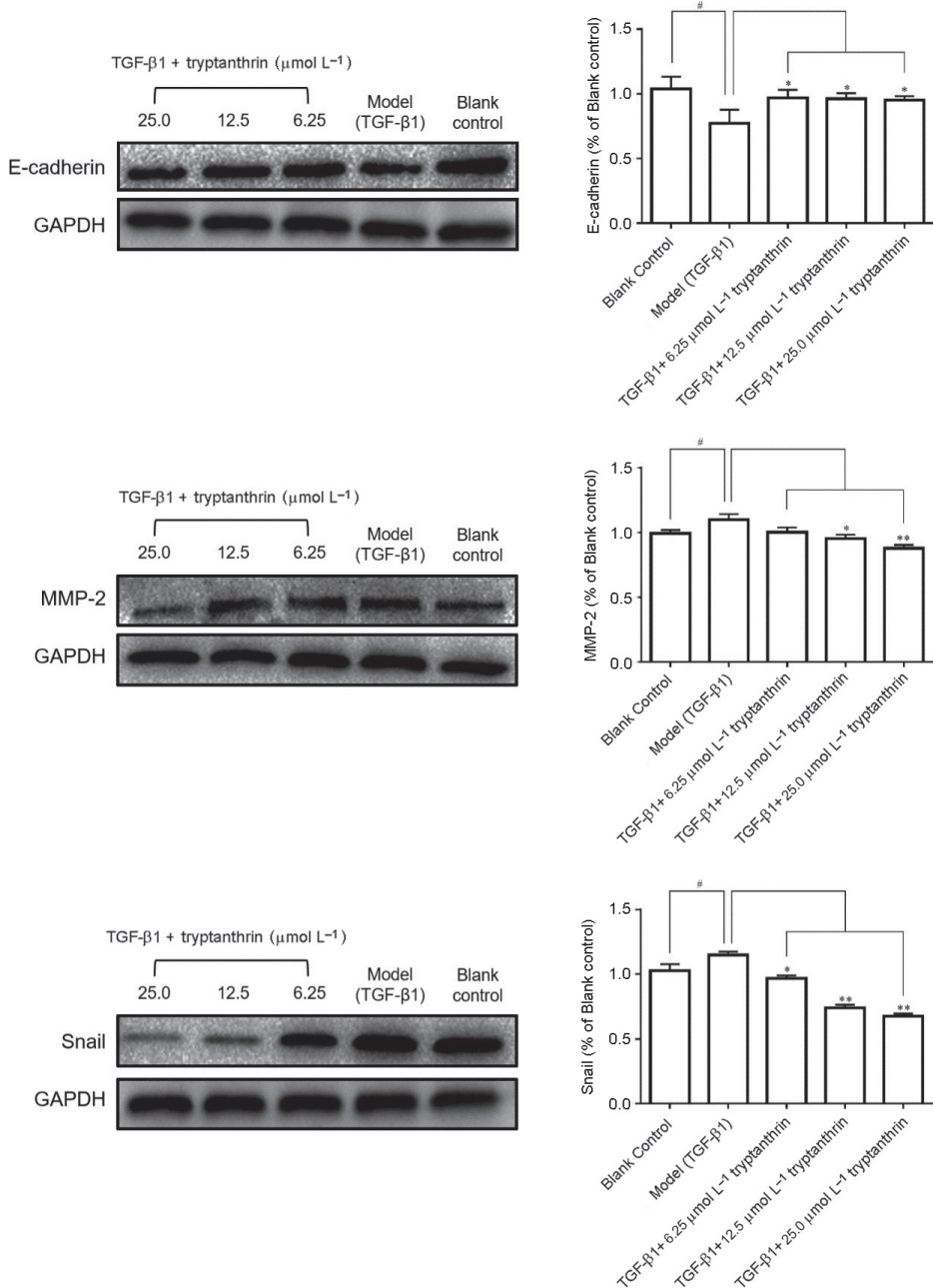


Fig. 5. The expression level of E-cadherin, MMP-2 and Snail proteins in MCF-7 tumor cells under the effect of tryptanthrin (compared to the blank control group, [#]*p* < 0.05; compared to the model group, **p* < 0.05, ***p* < 0.01, *n* = 3).

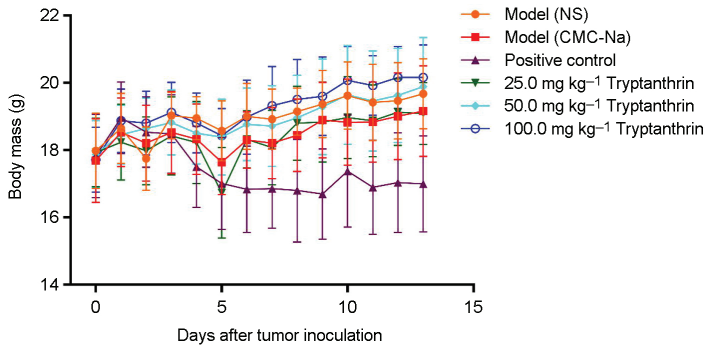


Fig. 6. Changes in the body mass of tumor-bearing mice under the effect of tryptanthrin ($n = 9$).

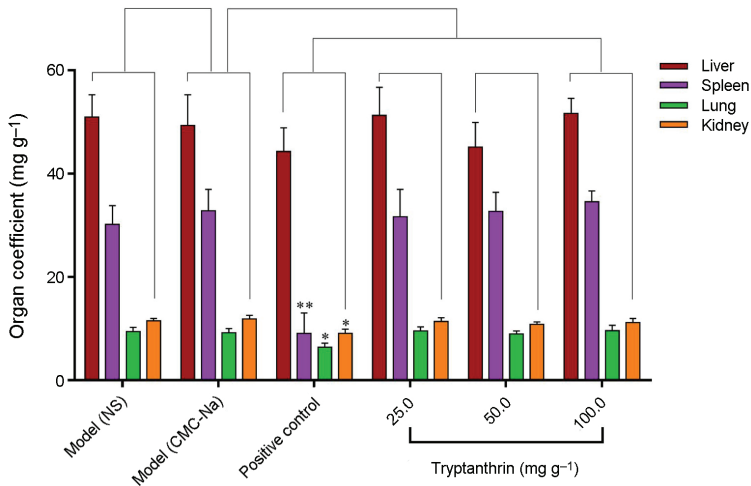


Fig. 7. Organ coefficients of tumor-bearing mice under the effect of tryptanthrin (compared to model group, * $p < 0.05$, ** $p < 0.01$, $n = 9$).

and IL-10 up-regulation is reported to be related to the poor patient prognosis which plays a promoting role in breast cancer (37, 38). The serum IL-6 and IL-12 levels in tumor-bearing mice of all experimental groups did not exhibit a significant trend (Fig. 9).

Tryptanthrin improved histopathological changes in organs and tumor tissues from tumor-bearing mice

Livers, lungs and spleens were dissected from tumor-bearing mice as the main organs to evaluate the therapeutic effect of tryptanthrin based on the H&E staining histopathological images. As shown in Fig. 10, the ratios of H&E staining in the organs of tryptanthrin-treated groups showed no significant differences relative to those in the normal control

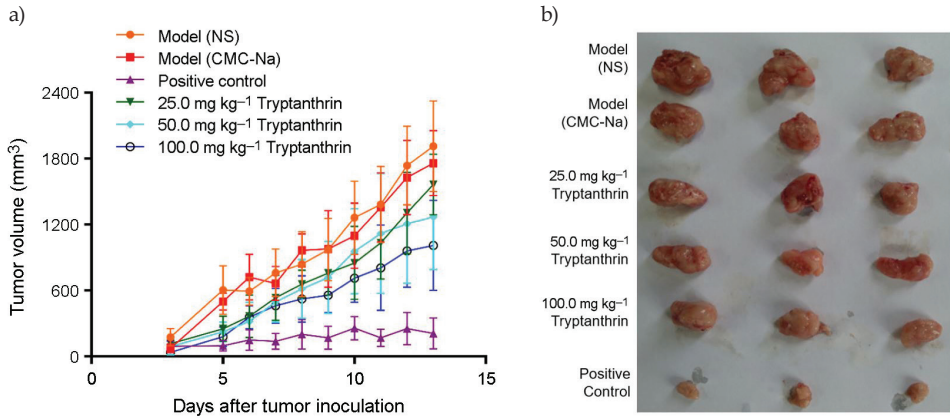


Fig. 8. a) The change curves of tumor volume and b) morphologic changes of breast tumor tissues of tumor-bearing mice under the effect of tryptanthrin ($n = 9$).

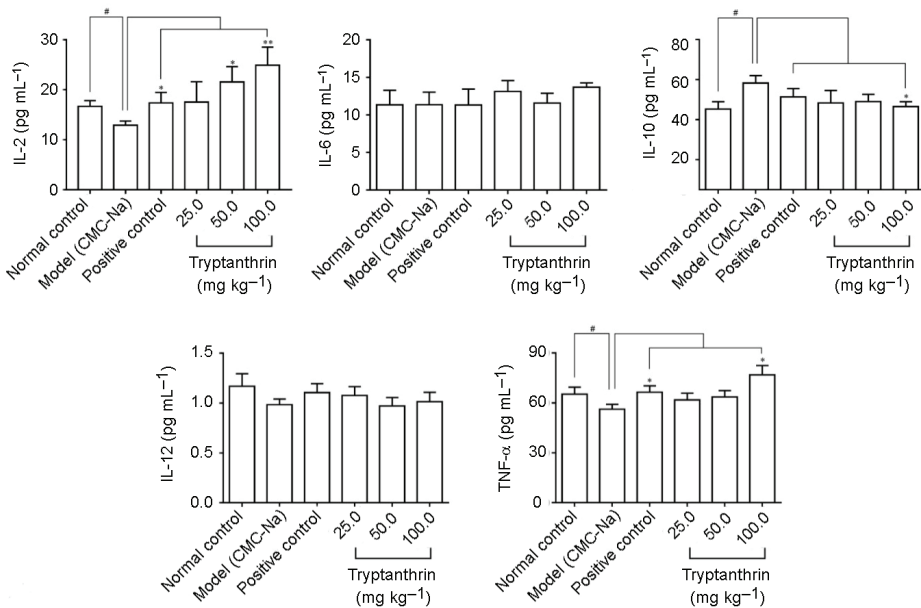


Fig. 9. Expression of IL-2, IL-6, IL-10, IL-12 and TNF- α in the serum of tumor-bearing mice (compared to the normal control group, [#] $p < 0.05$; compared to the model group, * $p < 0.05$, ** $p < 0.01$, $n = 3$).

group and the model group. The tumor in tumor-bearing mice of tryptanthrin-treated groups showed no difference to the tissue morphology of normal organs, and tryptanthrin treatments at 25.0–100.0 mg kg⁻¹ for once a day for 13 consecutive days had no obvious

toxic effects on these main organs in tumor-bearing mice. By contrast, tumor tissues in 25.0–100.0 mg kg⁻¹ tryptanthrin-treated groups were inhibited to various degrees (**p* < 0.05), suggesting that tryptanthrin had a favorable anti-breast cancer effect *in vivo*.

Tryptanthrin inhibited COX-2, NOS1 and NF-κB p65 in tumor tissues from tumor-bearing mice

IHC analysis demonstrated that the expression levels of COX-2 and NOS1 were down-regulated in tumor tissues from tumor-bearing mice treated with various doses of trypt-

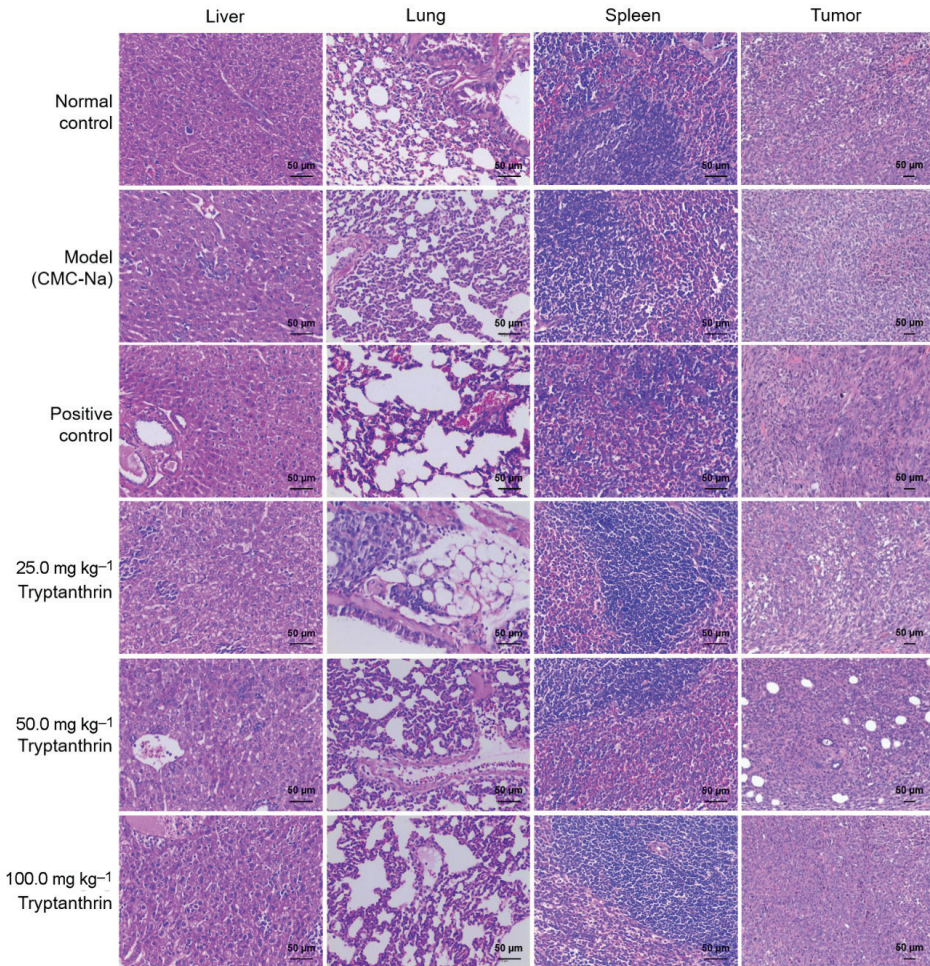


Fig. 10. HE-staining histopathological images of liver, spleen, lung tissues ($\times 400$) and tumor tissue ($\times 200$) of normal mice and tumor-bearing mice under the effect of tryptanthrin.

anthrin or the positive drug (Fig. 11). In the meantime, the expression of COX-2 in tumor-bearing mice treated with 100.0 mg kg⁻¹ tryptanthrin, and that of NOS1 in tumor-bearing mice treated with 25.0, 50.0, 100.0 mg kg⁻¹ tryptanthrin, were dramatically suppressed (**p* < 0.05). COX-2 is overexpressed in the metastatic process of all cancers, which is considered to be a marker of the dismal prognosis for breast cancer and lung cancer (39). Furthermore,

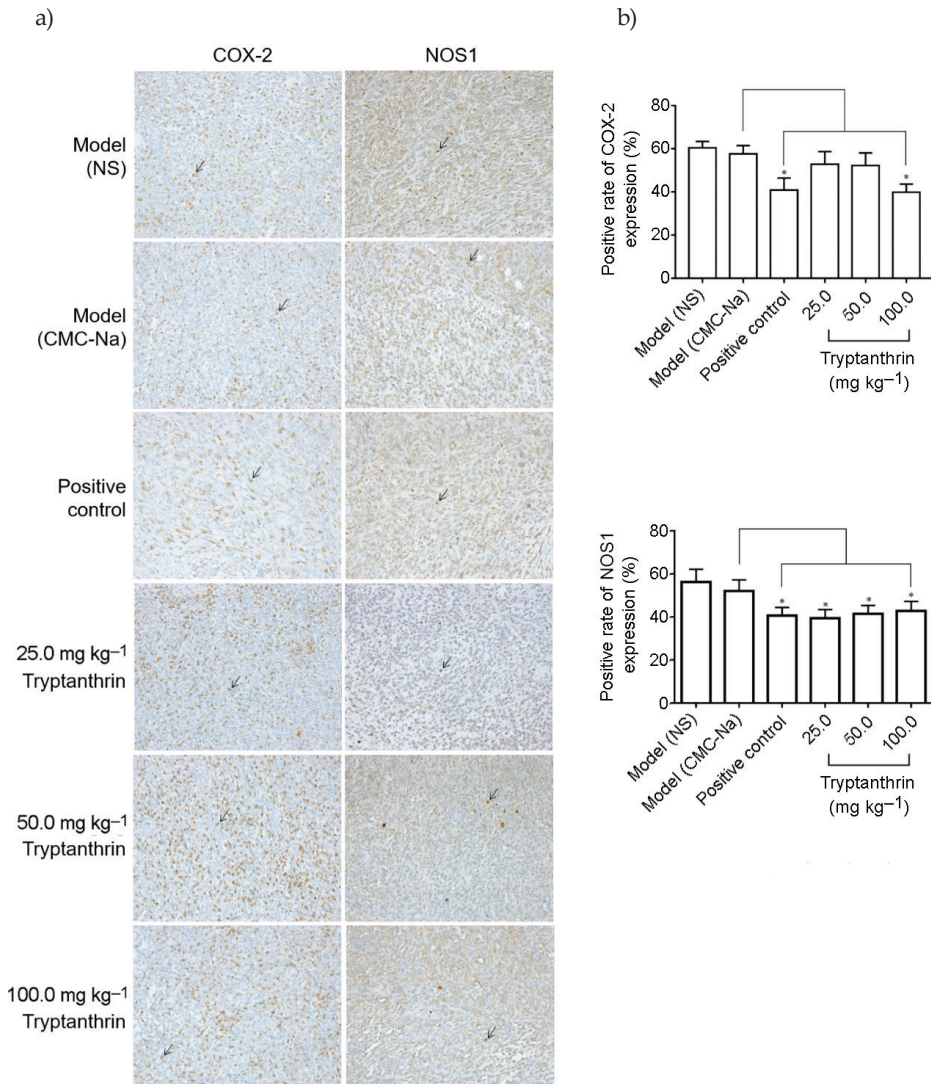


Fig. 11. a) Immunohistochemical staining diagrams and b) quantitative histograms of COX-2 and NOS1 protein expressions in tumor tissues of tumor-bearing mice ($\times 200$) (compared to the 0.5 % CMC-Na Model group, **p* < 0.05, *n* = 9).

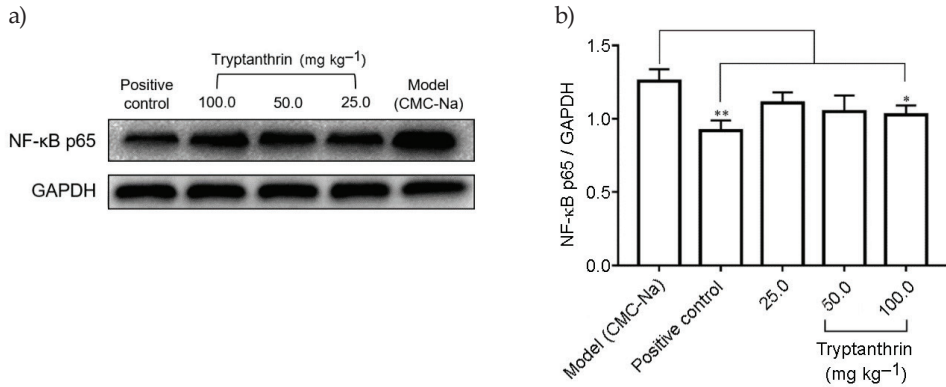


Fig. 12. Expression of NF-κB protein in tumor tissues of tumor-bearing mice (compared to the model group, * $p < 0.05$, $n = 3$).

the expression of NF-κB p65 in tumor tissues from tumor-bearing mice was analyzed through Western blotting, which was high in the model group, but low in the tryptanthrin-treated groups and the positive group (* $p < 0.05$, ** $p < 0.01$) (Fig. 12), indicating that tryptanthrin had downregulated NF-κB p65 protein expression in tumor-bearing mice. NF-κB, as a transcription factor that connects the molecular centers of inflammation and cancer, is recognized to trigger oncogenesis through activating the NF-κB cascades to enhance cell proliferation, suppress apoptosis, and promote cell invasion as well as metastasis (40, 41).

CONCLUSIONS

Breast cancer is a malignancy commonly seen among women worldwide. Human breast cancer MCF-7 cells are a kind of estrogen receptor-positive breast cancer cells. Breast cancer oncogenesis is related to the inflammatory tumor microenvironment (TME) (42, 43). In this study, we investigated the modulation of tryptanthrin on the TME both *in vitro* and *in vivo*, and the results demonstrated that tryptanthrin dramatically inhibited the proliferation of human breast cancer MCF-7 cells in a time- and concentration-dependent manner. Tryptanthrin treatment induced the poor adherence of MCF-7 cells, resulted in the darkened nuclei, the loss of cell membrane, and cytoplasm diffusion, indicating a change in the normal cell morphology. Tryptanthrin treatment not only inhibited the migration and invasion of MCF-7 cells, but also suppressed the TGF-β1-induced transition of MCF-7 cells, which played an important role in inducing epithelial-mesenchymal transition (EMT) *in vitro*. Tryptanthrin had also remarkably enhanced the expression levels of E-cadherin and depressed those of MMP-2 and Snail in MCF-7 cells stimulated by TGF-β1. This study demonstrated that tryptanthrin treatment inhibits the proliferation of breast cancer cells, and suppresses the TME-associated EMT induced by TGF-β1 treatment.

4T1 mouse breast cancer models were applied to evaluate *in vivo* anti-tumor effect of tryptanthrin. Body mass of mice administered with the positive drug was dramatically reduced, whereas in tumor-bearing mice from tryptanthrin treatment groups showed no marked difference, spleen organ coefficient in the positive group was the most signifi-

cantly reduced. Our results showed that tryptanthrin had considerable inhibitory activity on tumor growth in mice, much lower toxic and side effects on organisms than those of the positive drug cyclophosphamide. Serum expression levels of IL-6 and IL-12 in tumor-bearing mice from all groups were not significantly changed, and those of IL-2 and TNF- α in tumor-bearing mice from tryptanthrin groups were up-regulated. Compared to the normal control, the serum level of IL-10 in the model group had increased dramatically, whereas the levels in tumor-bearing mice treated with 100.0 mg kg⁻¹ tryptanthrin had decreased. Through histopathological examinations of organs and tumor tissues from tumor-bearing mice, it was found that the different doses of tryptanthrin groups partially inhibited the metastasis and apoptosis of organs and tumor tissues. In addition, the protein expression levels of COX-2, NOS1 and NF- κ B p65 in tumor tissues of tumor-bearing mice from tryptanthrin groups were notably downregulated, the expression levels of COX-2 and NOS1 are closely associated with the pro-inflammatory environment of breast cancer.

To sum up, findings of this study suggest that tryptanthrin inhibits the proliferation, migration and invasion of MCF-7 cells, which is partly achieved through the upregulation of protein levels of E-cadherin and downregulation of MMP-2 and Snail in MCF-7 cells *in vitro* compared to the normal physiological levels. Tryptanthrin also suppresses tumor growth in mice. The proposed pharmacological mechanism is downregulation of the NOS1, COX-2 and NF- κ B expression in mouse tumor tissues, upregulation of IL-2 and TNF- α , and recovery of the serum IL-10 levels in mice bearing tumor cells. In conclusion, tryptanthrin exerts its anti-breast cancer activities through modulating the inflammatory TEM both *in vitro* and *in vivo*.

Acronyms, abbreviations, symbols. – CMC-Na – sodium carboxymethyl cellulose, H&E – hematoxylin and eosin, ELISA – enzyme-linked immunosorbent assay, EMT – epithelial-mesenchymal transition, IHC – immunohistochemistry, TNF- α – tumor necrosis factor α , TME – tumor microenvironment, HRP – horseradish peroxidase.

Acknowledgements. – This work was financially supported by Guizhou Provincial Natural Science Foundation (2020-1Y404), NSFC-Guizhou Karst Scientific Research Center (U1812403), International S&T Cooperation Base for Pharmacy in Guizhou Medical University (2017-5802), Reform Project of Undergraduate Teaching Content and Course System of Guizhou Medical University (2019-60), Guizhou Provincial Innovation and Entrepreneurship Training Project for College Students (No. 201510660024) and Doctoral Fund of Guizhou Medical University (No. J[2014]006).

Supplementary material available upon request.

REFERENCES

1. A. H. N. Kamdje, P. F. S. Etet, L. Vecchio, J. M. Muller, M. Krampera and K. E. Lukong, Signaling pathways in breast cancer: Therapeutic targeting of the microenvironment, *Cell. Signal.* **26** (2014) 2843–2856; <https://doi.org/10.1016/j.cellsig.2014.07.034>
2. K. Velaei, N. Samadi, B. Barazvan and J. S. Rad, Tumor microenvironment-mediated chemoresistance in breast cancer, *The Breast* **30** (2016) 92–100; <https://doi.org/10.1016/j.breast.2016.09.002>
3. Q. J. Guo, J. Li and H. S. Lin, Effect and molecular mechanisms of traditional chinese medicine on regulating tumor immunosuppressive microenvironment, *BioMed Res. Int.* **2015** (2015) 261620; <https://doi.org/10.1155/2015/261620>
4. M. Pesic and F. R. Greten, Inflammation and cancer: tissue regeneration gone awry, *Curr. Opin. Cell. Biol.* **43** (2016) 55–61; <https://doi.org/10.1016/j.ceb.2016.07.010>

5. M. Suarez-Carmona, J. Lesage, D. Cataldo and C. Gilles, EMT and inflammation: inseparable actors of cancer progression, *Mol. Oncol.* **11** (2017) 805–823; <https://doi.org/10.1002/1878-0261.12095>
6. X. Y. Li, L. Su, Y. M. Jiang, W. B. Gao, C. W. Xu, C. Q. Zeng, J. Song, Y. Xu, W. C. Weng and W. B. Liang, The antitumor effect of xihuang pill on treg cells decreased in tumor microenvironment of 4T1 breast tumor-bearing mice by PI3K/AKT-AP-1 signaling pathway, *Evid.-Based Compl. Alt. Med.* **2018** (2018) 6714829; <https://doi.org/10.1155/2018/6714829>
7. F. R. Balkwill and A. Mantovani, Cancer-related inflammation: Common themes and therapeutic opportunities, *Semin. Cancer Biol.* **22** (2012) 33–40; <https://doi.org/10.1016/j.semcancer.2011.12.005>
8. Z. T. Li, Y. J. Zhu, C. C. Li, R. Trinh, X. Y. Ren, F. M. Sun, Y. F. Wang, P. Z. Shang, T. Wang, M. Wang, S. L. Morrison and J. Zhang, Anti-VEGFR2-interferon- α 2 regulates the tumor microenvironment and exhibits potent antitumor efficacy against colorectal cancer, *Oncoimmunology* **6** (2017) e1290038; <https://doi.org/10.1080/2162402X.2017.1290038>
9. F. L. Bai, Z. S. Niu, H. Tian, S. M. Li, Z. Lv, T. Y. Zhang, G. P. Ren and D. S. Li, Genetically engineered Newcastle disease virus expressing interleukin 2 is a potential drug candidate for cancer immunotherapy, *Immunol. Lett.* **159** (2014) 36–46; <https://doi.org/10.1016/j.imlet.2014.02.009>
10. T. van der Heijden, I. Bot and J. Kuiper, The IL-12 cytokine family in cardiovascular diseases, *Cytokine* **122** (2019) 154188; <https://doi.org/10.1016/j.cyto.2017.10.010>
11. K. Singh, M. Roy, P. Prajapati, A. Lipatova, L. Sripada, D. Gohel, A. Singh, M. Mane, M. M. Godbole, P. M. Chumakov and R. Singh, NLRX1 regulates TNF- α -induced mitochondria-lysosomal crosstalk to maintain the invasive and metastatic potential of breast cancer cells, *BBA-Mol. Basis Dis.* **1865** (2019) 1460–1476; <https://doi.org/10.1016/j.bbadis.2019.02.018>
12. K. A. Silverio and S. A. Patel, Harnessing antitumor immunity: Employment of tumor recall antigens to optimize the inflammatory response to cancer (Review), *Oncol. Lett.* **13** (2017) 2015–2020; <https://doi.org/10.3892/ol.2017.5721>
13. S. Suman, P. K. Sharma, G. Rai, S. Mishra, D. Arora, P. Gupta and Y. Shukla, Current perspectives of molecular pathways involved in chronic inflammation-mediated breast cancer, *Biochem. Bioph. Res. Commun.* **472** (2016) 401–409; <https://doi.org/10.1016/j.bbrc.2015.10.133>
14. I. Uehara and N. Tanaka, Role of p53 in the regulation of the inflammatory tumor microenvironment and tumor suppression, *Cancers* **10** (2018) 219; <https://doi.org/10.3390/cancers10070219>
15. J. F. Lima, S. Nofech-Mozes, J. Bayani and J. M. S. Bartlett, EMT in breast carcinoma – A review, *J. Clin. Med.* **5** (2016) 65; <https://doi.org/10.3390/jcm5070065>
16. L. Yan, F. Xu and C. L. Dai, Relationship between epithelial-to-mesenchymal transition and the inflammatory microenvironment of hepatocellular carcinoma, *J. Exp. Clin. Cancer Res.* **37** (2018) 203; <https://doi.org/10.1186/s13046-018-0887-z>
17. L. EL-Hajjar, N. Jalaliddine, A. Shaito, K. Zibara, J. M. Kazan, J. El-Saghir and M. El-Sabban, Bevacizumab induces inflammation in MDA-MB-231 breast cancer cell line and in a mouse model, *Cell. Signal.* **53** (2019) 400–412; <https://doi.org/10.1016/j.cellsig.2018.11.007>
18. H. N. Chang, S. T. Huang, Y. C. Yeh, H. S. Wang, T. H. Wang, Y. H. Wu and J. S. Pang, Indigo naturalis and its component tryptanthrin exert anti-angiogenic effect by arresting cell cycle and inhibiting Akt and FAK signaling in human vascular endothelial cells, *J. Ethnopharmacol.* **174** (2015) 474–481; <https://doi.org/10.1016/j.jep.2015.08.050>
19. S. L. Hsuan, S. C. Chang, S. Y. Wang, T. L. Liao, T. T. Jong, M. S. Chien, W. C. Lee, S. S. Chen and J. W. Liao, The cytotoxicity to leukemia cells and antiviral effects of *isatis indigotica* extracts on pseudorabies virus, *J. Ethnopharmacol.* **123** (2009) 61–67; <https://doi.org/10.1016/j.jep.2009.02.028>
20. Y. H. Liang, H. X. Hou, D. R. Li, J. Qin, L. Qiu and H. H. Wu, Studies on *in vitro* anticancer activity of tryptanthrin B, *Chin. Tradit. Herbal Drugs* **31** (2000) 531–533; <https://doi.org/10.3321/j.issn:0253-2670.2000.07.029>
21. J. P. Li, G. H. Zhu, Y. Yuan and M. X. Liu, Anti-tumor and immune function regulation effects of *radix isatidis* polysaccharides *in vivo*, *Nat. Prod. Res. Dev.* **29** (2017) 2010–2016; <https://doi.org/10.16333/j.1001-6880.2017.12.003>

22. L. L. Liu, J. Chen and Y. P. Shi, Advances in studies on antitumor of Chinese materia medica with heat-clearing and toxin-resolving functions, *Chin. Tradit. Herbal Drugs* **43** (2012) 1203–1212; <https://www.cqvip.com/qk/80172x/201211/42183551.html>
23. G. Honda and M. Tabata, Isolation of antifungal principle tryptanthrin, from *Strobilanthes Cusia* O. Kuntze, *Planta Med.* **36** (1979) 85–86; <https://doi.org/10.1055/s-0028-1097245>
24. R. Kaur, S. K. Manjal, R. K. Rawal and K. Kumar, Recent synthetic and medicinal perspectives of tryptanthrin, *Bioorg. Med. Chem.* **25** (2017) 4533–4552; <https://doi.org/10.1016/j.bmc.2017.07.003>
25. E. H. Jung, J. Y. Jung, H. L. Ko, J. K. Kim, S. M. Park, D. H. Jung, C. A. Park, Y. W. Kim, S. K. Ku, I. J. Cho and S. C. Kim, Tryptanthrin prevents oxidative stress-mediated apoptosis through AMP-activated protein kinase-dependent p38 mitogen-activated protein kinase activation, *Arch. Pharm. Res.* **40** (2017) 1071–1086; <https://doi.org/10.1007/s12272-017-0947-5>
26. S. Lee, D. C. Kim, H. Y. Baek, K. D. Lee, Y. C. Kim and H. Oh, Anti-neuroinflammatory effects of tryptanthrin from *Polygonum tinctorium* Lour. in lipopolysaccharide-stimulated BV2 microglial cells, *Arch. Pharm. Res.* **41** (2018) 419–430; <https://doi.org/10.1007/s12272-018-1020-8>
27. S. T. Yu, J. W. Chern, T. M. Chen, Y. F. Chiu, H. T. Chen and Y. H. Chen, Cytotoxicity and reversal of multidrug resistance by tryptanthrin-derived indoloquinazolines, *Acta Pharmacol. Sin.* **31** (2010) 259–264; <https://doi.org/10.1038/aps.2009.198>
28. Y. W. Kwon, S. Y. Cheon, S. Y. Park, J. Song and J. H. Lee, Tryptanthrin suppresses the activation of the LPS-treated BV2 microglial cell line via Nrf2/HO-1 antioxidant signaling, *Front Cell Neurosci.* **11** (2017) 18; <https://doi.org/10.3389/fncel.2017.00018>
29. M. J. Micallef, K. Iwaki, T. Ishihara, S. Ushio, M. Aga, T. Kunikata, S. Koya-Miyata, T. Kimoto, M. Ikeda and M. Kurimoto, The natural plant product tryptanthrin ameliorates dextran sodium sulfate-induced colitis in mice, *Int. Immunopharmacol.* **2** (2002) 565–578; [https://doi.org/10.1016/S1567-5769\(01\)00206-5](https://doi.org/10.1016/S1567-5769(01)00206-5)
30. R. Kaur, S. K. Manjal, R. K. Rawal and K. Kumar, Recent Synthetic and Medicinal Perspectives of Tryptanthrin, *Bioorg. Med. Chem.* **25** (2017) 4533–4552; <https://doi.org/10.1016/j.bmc.2017.07.003>
31. W. Zhou, Q. F. Zeng, D. Lai, J. L. Cho, X. Y. Zhang and X. C. Shen, Effect of tryptanthrin on proliferation of human breast cancer MCF-7 cells via MAPK signaling pathway, *Chin. Pharm. J.* **54** (2019) 693–698; <https://doi.org/10.11669/cpj.2019.09.005>
32. X. M. Liao and K. N. Leung, Tryptanthrin induces growth inhibition and neuronal differentiation in the human neuroblastoma LA-N-1 cells, *Chem. Biol. Interact.* **203** (2013) 512–521; <https://doi.org/10.1016/j.cbi.2013.03.001>
33. S. Han, D. F. Li, C. M. Wu, X. R. Ma, R. G. Song and Y. Wang, Synthesis and characterization of indoloquinazoline derivatives, *Chem. Reagents* **33** (2011) 883–886; <https://doi.org/10.13822/j.cnki.hxsj.2011.10.011>
34. J. H. Feng, D. L. Song, S. Y. Jiang, X. H. Yang, T. T. Ding, H. Zhang, J. M. Luo, J. Liao and Q. Yin, Quercetin restrains TGF- β 1-induced epithelial–mesenchymal transition by inhibiting Twist1 and regulating E-cadherin expression, *Biochem. Biophys. Res. Commun.* **498** (2018) 132–138; <https://doi.org/10.1016/j.bbrc.2018.02.044>
35. M. Mizui, Natural and modified IL-2 for the treatment of cancer and autoimmune diseases, *Clin. Immunol.* **206** (2019) 63–70; <https://doi.org/10.1016/j.clim.2018.11.002>
36. A. Tang and F. Harding, The challenges and molecular approaches surrounding interleukin-2-based therapeutics in cancer, *Cytokine: X* **1** (2019) 100001; <https://doi.org/10.1016/j.cyttox.2018.100001>
37. X. G. Li, P. Lu, B. Li, W. F. Zhang, R. Yang, Y. Chu and K. Y. Luo, Interleukin 2 and interleukin 10 function synergistically to promote CD8⁺ T cell cytotoxicity, which is suppressed by regulatory T cells in breast cancer, *Int. J. Biochem. Cell Biol.* **87** (2017) 1–7; <https://doi.org/doi:10.1016/j.biocel.2017.03.003>
38. M. H. Mannino, Z. W. Zhu, H. P. Xiao, Q. Bai, M. R. Wakefield and Y. J. Fang, The paradoxical role of IL-10 in immunity and cancer, *Cancer Lett.* **367** (2015) 103–107; <https://doi.org/10.1016/j.canlet.2015.07.009>

39. R. Liu, H. G. Zheng, W. D. Li, Q. J. Guo, S. L. He, Y. Hirasaki, W. Hou, B. J. Hua, C. H. Li, Y. J. Bao, Y. B. Gao, X. Qi, Y. X. Pei and Y. Zhang, Anti-tumor enhancement of Fei-Liu-Ping ointment in combination with celecoxib via cyclooxygenase-2-mediated lung metastatic inflammatory microenvironment in Lewis lung carcinoma xenograft mouse model, *J. Transl. Med.* **13** (2015) 366; <https://doi.org/10.1186/s12967-015-0728-1>
40. D. Capece, D. Verzella, A. Tessitore, E. Alesse, C. Capalbo and F. Zazzeroni, Cancer secretome and inflammation: The bright and the dark sides of NF- κ B, *Semin. Cell Dev. Bio.* **78** (2018) 51–61; <https://doi.org/10.1016/j.semcdb.2017.08.004>
41. M. Patel, P. G. Horgan, D. C. McMillan and J. Edwards, NF- κ B pathways in the development and progression of colorectal cancer, *Transl. Res.* **197** (2018) 43–56; <https://doi.org/10.1016/j.trsl.2018.02.002>
42. M. Egue, F. H. R. Gnangnon, M. T. Akele-Akpo and D. M. Parkin, Cancer incidence in Cotonou (Benin), 2014–2016 First results from the cancer Registry of Cotonou, *Cancer Epidemiol.* **59** (2019) 46–50; <https://doi.org/10.1016/j.canep.2019.01.006>
43. L. Su, Y. M. Jiang, Y. Xu, X. Y. Li, W. B. Gao, C. W. Xu, C. Q. Zeng, J. Song, W. C. Weng and W. B. Liang, Xihuang pill promotes apoptosis of Treg cells in the tumor microenvironment in 4T1 mouse breast cancer by upregulating MEKK1/SEK1/JNK1/AP-1 pathway, *Biomed. Pharmacother.* **102** (2018) 1111–1119; <https://doi.org/10.1016/j.biopha.2018.03.063>